

# Tensor polarization and spectral properties of vector meson in QCD medium

Feng Li<sup>1,2,3,4,\*</sup> and Shuai Y.F. Liu<sup>5,6,7,†</sup>

<sup>1</sup>*School of Physical Science and Technology, Lanzhou University, Lanzhou 730000, China*

<sup>2</sup>*Research Center for Hadron and CSR Physics, Lanzhou University  
and Institute of Modern Physics of CAS, Lanzhou 730000, China*

<sup>3</sup>*Lanzhou Center for Theoretical Physics, Key Laboratory of Theoretical Physics of Gansu Province,  
and Frontiers Science Center for Rare Isotopes, Lanzhou University, Lanzhou 730000, China*

<sup>4</sup>*Frontiers Science Center for Rare Isotopes, Lanzhou University*

<sup>5</sup>*School of Physics and Electronics, Hunan University, Changsha 410082, China*

<sup>6</sup>*Hunan Provincial Key Laboratory of High-Energy Scale Physics and Applications, Hunan University, Changsha 410082, China*

<sup>7</sup>*Quark Matter Research Center, Institute of Modern Physics,  
Chinese Academy of Sciences, Lanzhou 730000, China*

(Dated: March 12, 2024)

We calculate the tensor polarization and the resulted spin alignment of a generic vector meson in local equilibrium up to the first order in hydrodynamic gradients using thermal field theory with dissipative effects incorporated. Several new contributions, including a novel shear-induced tensor polarization (SITP), are discovered and turn out sensitive to the in-medium spectral properties of the vector mesons. The phenomenological study reveals that these contributions, especially SITP, could generate substantial spin alignment in heavy-ion collisions, and potentially helps us to understand the large spin alignment observed in experiments.

*Introduction.*—Tensor polarization of spin-1 bosons plays vital roles in many branches of physics [1]. For example, tensor polarization related observables in electron-deuteron scattering experiments are utilized to probe the features of nuclear interaction [2–5]. In the context of the high energy  $e^+e^-$  and  $pp$  collisions, the measurement of vector meson’s tensor polarization is employed for investigating the spin-dependent fragmentation functions and hence the hadronization mechanism in QCD [6, 7]. In heavy-ion collisions (HICs), the spin-related physics is mostly studied in the context of hyperons’ vector polarization, from both experimental [8–12] and theoretical [13–25] perspectives. However, recently, motivated by pioneering works [13, 26–28], tensor polarizations of vector mesons produced in HICs, including  $K^*$ ,  $\phi$  and  $J/\Psi$  have been explored at both RHIC and LHC via analyzing spin alignment observables  $\delta\rho_{00}$  [29–33], where intriguing phenomena are discovered.

While substantial spin alignment has been observed for vector mesons mentioned above, the theoretical descriptions are much smaller than the data and are difficult to accommodate the sign changes of  $\delta\rho_{00}$  [28, 34–36], since the predicted spin alignment is proportional to the square of the vorticity. Efforts have been made from the other perspectives [37–40] to reveal the mechanism of the spin alignment of the vector mesons as well. But the origin of the spin alignment is still considered as an open question [36]. Besides the theoretical descriptions mentioned above, a systematic calculation under the framework of thermal field theory, which has achieved notable progresses [20–23] in solving the “spin sign puzzles” of  $\Lambda$ -hyperon [11, 41], seems to be missing in studying the spin alignment at this moment. In this work, we have developed the first thermal field framework for calculating the tensor polarization and the spin alignment, in which a

novel shear-induced-tensor polarization (SITP) is discovered as a significant contribution to the spin alignment and found sensitive to the spectral properties of the vector bosons.

*Theoretical framework.*—We begin by introducing the *Wigner functions* of a massive vector meson with mass  $m$  and field operator  $V^\mu$ :

$$\begin{aligned} W^{\mu\nu}(x, \mathbf{p}) &\equiv \varepsilon_{\mathbf{p}} \int dp^0 \int d^4y e^{ip \cdot y} \langle V^\mu(x_-) V^\nu(x_+) \rangle \\ &= W_+^{\mu\nu}(x, \mathbf{p}) + W_-^{\mu\nu}(x, \mathbf{p}) \end{aligned} \quad (1)$$

where  $x_\pm = x \pm y/2$ ,  $\varepsilon_{\mathbf{p}} = \sqrt{\mathbf{p}^2 + m^2}$ ,  $\langle \dots \rangle$  denotes the thermal ensemble average, and  $W_\pm$  denote the integration over the positive and negative  $p^0$  respectively, corresponding to the differential spin density matrix  $\varrho(x, \pm\mathbf{p})$  [14], where the  $\varrho(x, \mathbf{p})$  is embedded in Wigner function as

$$\begin{aligned} 2W_+^{\mu\nu}(x, \mathbf{p}) &= \sum_{s, s'} \epsilon_s^{\mu*}(\mathbf{p}) \epsilon_{s'}^\nu(\mathbf{p}) \varrho_{s's}(x, \mathbf{p}) + \delta W^{\mu\nu} \\ &\equiv \mathcal{W}^{\mu\nu}(x, \mathbf{p}) + \delta W^{\mu\nu}(x, \mathbf{p}). \end{aligned} \quad (2)$$

The factor “2” is for matching the conventional normalization of the density matrix. The  $\epsilon_s(\mathbf{p})$  represents the polarization vector of the vector meson moving with momentum  $\mathbf{p}$  and occupying the spin state  $s$ , and satisfies  $\tilde{p} \cdot \epsilon_s(\mathbf{p}) = 0$  with  $\tilde{p} = (\varepsilon_{\mathbf{p}}, \mathbf{p})$  being the on-shell 4-momentum. So, the projected Wigner function

$$\mathcal{W}^{\mu\nu}(x, \mathbf{p}) \equiv \sum_{s, s'} \epsilon_s^{\mu*}(\mathbf{p}) \epsilon_{s'}^\nu(\mathbf{p}) \varrho_{s's}(x, \mathbf{p}) \quad (3)$$

is perpendicular to the on-shell 4-momentum  $\tilde{p}$  as well, and can therefore be expressed as

$$\mathcal{W}^{\mu\nu}(x, \mathbf{p}) \equiv 2\tilde{\Delta}_\alpha^\mu \tilde{\Delta}_\beta^\nu W_+^{\alpha\beta}(x, \mathbf{p}) \quad (4)$$

where  $\tilde{\Delta}$  is the shorthand of  $\Delta(\tilde{p})$  with  $\Delta^{\mu\nu}(p) \equiv -\eta^{\mu\nu} + p^\mu p^\nu/p^2$  being the projector with respect to a 4-momentum  $p$  (note  $\Delta^2 = -\Delta$ ). The  $\delta W$  can always be chosen vanishing after projections. Conversely, the differential spin-density matrix can be evaluated via the projected Wigner function as [42]

$$\varrho_{ss'}(x, \mathbf{p}) = \epsilon_{s'}^\mu(\mathbf{p}) \epsilon_s^{\nu*}(\mathbf{p}) \mathcal{W}_{\mu\nu}(x, \mathbf{p}). \quad (5)$$

The projected Wigner function can be further decomposed, according to the representation of the rotational symmetry, into three parts as

$$\mathcal{W}^{\mu\nu} = \frac{1}{3} \tilde{\Delta}^{\mu\nu} \mathcal{S} + \mathcal{W}^{[\mu\nu]} + \mathcal{T}^{\mu\nu} \quad (6)$$

where  $\mathcal{S} \equiv \mathcal{W}^{\mu\nu} \tilde{\Delta}_{\mu\nu}$  is the 3D trace of  $\mathcal{W}^{\mu\nu}$  and related to spin-summed phase space density,  $W^{[\mu\nu]} \equiv (W^{\mu\nu} - W^{\nu\mu})/2$  corresponds to the vector polarization of the vector meson, and  $\mathcal{T}^{\mu\nu}$  defined as

$$\mathcal{T}^{\mu\nu} \equiv \mathcal{W}^{(\mu\nu)} \equiv \mathcal{W}^{(\mu\nu)} - \frac{1}{3} \tilde{\Delta}^{\mu\nu} \mathcal{S} = 2 \tilde{\Delta}_\lambda^{(\mu} \tilde{\Delta}_\nu^{\lambda)} W_+^{(\lambda\gamma)} \quad (7)$$

corresponds to the tensor polarization of the vector field, which is of the major interest in this work. Here, the round bracket “(...)” stands for symmetrizing the included space-time indices, i.e.,  $W^{(\mu\nu)} = (W^{\mu\nu} + W^{\nu\mu})/2$ , while the angle bracket “ $\langle \dots \rangle$ ” stands for further making the tensor traceless about the included indices.

$\mathcal{T}^{\mu\nu}$  can be further expanded in terms of the hydrodynamic gradients as

$$\mathcal{T}^{\mu\nu} \approx \mathcal{T}_{(0)}^{\mu\nu} + \mathcal{T}_{(1)}^{\mu\nu} = 2 \tilde{\Delta}_\lambda^{(\mu} \tilde{\Delta}_\nu^{\lambda)} \left( W_{+(0)}^{(\lambda\gamma)} + W_{+(1)}^{(\lambda\gamma)} \right) \quad (8)$$

where the subscripts (0) and (1) stand for the zeroth and first order of the hydrodynamic gradients (or  $\partial$ ). After listing all the symmetry-allowed tensor structures non-vanishing under the projection  $\tilde{\Delta}_\lambda^{(\mu} \tilde{\Delta}_\nu^{\lambda)}$  up to the order of  $\partial$ , we further express  $\mathcal{T}^{\mu\nu}$  schematically as

$$\mathcal{T}^{\mu\nu} = \tilde{\Delta}_\lambda^{(\mu} \tilde{\Delta}_\nu^{\lambda)} \left[ \kappa_0^u u^\lambda u^\gamma + \kappa_1^u u^\lambda u^\gamma + \kappa_{\text{sh}} \sigma^{\lambda\gamma} + \kappa_T u^{(\lambda} \partial_\perp^{\gamma)} \beta + \kappa_{\text{su}} u^{(\lambda} \sigma^{\gamma)} \tilde{p}_\alpha + \kappa_{\text{ou}} u^{(\lambda} \Omega^{\gamma)} \alpha \tilde{p}_\alpha + \dots \right], \quad (9)$$

where  $u^\mu$  is the flow velocity and  $\beta = 1/T$  is the inverse temperature.  $\partial_\perp^\mu \equiv \tilde{\Delta}^{\mu\nu} \partial_\nu$  is the transverse derivative with the flow projector  $\tilde{\Delta}^{\mu\nu} \equiv \eta^{\mu\nu} - u^\mu u^\nu$ . The shear stress tensor is defined as  $\sigma^{\mu\nu} \equiv \partial_\perp^{(\mu} u^{\nu)}$   $-(1/3) \tilde{\Delta}^{\mu\nu} \theta$  with bulk stress  $\theta \equiv \partial \cdot u$ .  $\Omega^{\mu\nu} \equiv \partial_\perp^{[\mu} u^{\nu]}$  is vorticity. The SITP contribution  $\kappa_{\text{sh}} \sigma^{\lambda\gamma}$  appears naturally in this symmetry analysis with a T-odd coefficient  $\kappa_{\text{sh}}$  that should be originated from the dissipative processes. In the following, the  $\kappa$ -coefficients will be evaluated near thermal equilibrium under the framework of thermal field theory and linear response theory, with inclusion of dissipative physics.

The *zeroth-order term*  $\mathcal{T}_{(0)}^{\mu\nu}$  in Eq.(8) can be evaluated under exact/global thermal equilibrium and is related to the in-medium spectral function “ $A$ ” via

$$\begin{aligned} \mathcal{T}_{(0)}^{\mu\nu} &= 2 \tilde{\Delta}_\alpha^{(\mu} \tilde{\Delta}_\beta^{\nu)} \int_0^\infty dp^0 \int d^4 y e^{i p \cdot y} \langle V^\alpha(x_-) V^\beta(x_+) \rangle \\ &= 2 \tilde{\Delta}_\alpha^{(\mu} \tilde{\Delta}_\beta^{\nu)} \int_0^\infty dp^0 n(p^0) A^{\alpha\beta}(p), \end{aligned} \quad (10)$$

where  $n(\omega) = 1/(e^{\beta\omega} - 1)$  is the Bose-Einstein distribution. In the thermal medium, the longitudinal and transverse modes of the vector meson are different, so that the spectral function can be decomposed as [43, 44]

$$A^{\mu\nu} = \sum_{a=L,T} \Delta_a^{\mu\nu} A_a, \quad A_a = \frac{1}{\pi} \text{Im} \frac{-1}{p^2 - m^2 - \Pi_a}. \quad (11)$$

The longitudinal and transverse projector  $\Delta_{T,L}$  are  $\Delta_L^{\mu\nu} = v^\mu v^\nu / (-v^2)$ ,  $\Delta_T^{\mu\nu} = \Delta^{\mu\nu} - \Delta_L^{\mu\nu}$ , where  $v^\mu = \Delta^{\mu\nu} u_\nu$  is the projected flow velocity with respect to  $p$ . The on-shell version of these projectors are denoted by  $\tilde{\Delta}_L^{\mu\nu} = \tilde{v}^\mu \tilde{v}^\nu / (-\tilde{v}^2)$  with  $\tilde{v}^\mu = \tilde{\Delta}^{\mu\nu} u_\nu$  and  $\tilde{\Delta}_T^{\mu\nu} = \Delta_T^{\mu\nu}$ . Given that  $\tilde{\Delta}_\lambda^{(\mu} \tilde{\Delta}_\nu^{\lambda)} \Delta_L^{\lambda\gamma}(p) = \tilde{\Delta}_L^{\mu\nu} (1 - \Delta\omega^2 \tilde{v}^2/p^2)$  with  $\Delta\omega = p^0 - \varepsilon_{\mathbf{p}}$ , we therefore obtain that

$$\begin{aligned} \mathcal{T}_{(0)}^{\mu\nu} &= \alpha_0 n(\varepsilon_{\mathbf{p}}) \tilde{\Delta}_L^{(\mu\nu)} = \frac{\alpha_0}{-\tilde{v}^2} n(\varepsilon_{\mathbf{p}}) \tilde{\Delta}_\lambda^{(\mu} \tilde{\Delta}_\nu^{\lambda)} u^\lambda u^\gamma, \\ \alpha_0 &= 2\varepsilon_{\mathbf{p}} \int_0^\infty d\omega \frac{n(\omega)}{n(\varepsilon_{\mathbf{p}})} \left[ (A_L - A_T) - \frac{\Delta\omega^2 \tilde{v}^2}{p^2} A_L \right]. \end{aligned} \quad (12)$$

$A_L$  usually has a factor proportional to  $p^2$  cancelling with  $1/p^2$  to make the integration convergent. In principle, the  $\alpha_0$  in Eq. (12) should be evaluated numerically using a realistic in-medium spectral function. However, if we assume a non-analytic real energy shift at zero width limit,  $\alpha_0 \approx (\omega_{\mathbf{p}}^T - \omega_{\mathbf{p}}^L)/T$  where  $\omega_{\mathbf{p}}^{L/T}$  satisfying  $(\omega_{\mathbf{p}}^{L/T})^2 - \varepsilon_{\mathbf{p}}^2 - \text{Re}\Pi_{L/T}(\omega_{\mathbf{p}}^{L/T}, \mathbf{p}) = 0$  represents the shifted dispersion relation of the longitudinal and the transverse modes, respectively.

In the medium rest frame, nonzero momentum  $\mathbf{p}$  breaks the rotational symmetry, which results in the difference between  $A_L$  and  $A_T$  and therefore leads to the tensor polarization even in the absence of hydrodynamic gradient as expressed by the first term in  $\alpha_0$  in Eq. (12). Such splitting induced polarizations have also been discussed for virtual photons [45, 46]. In addition, the projection of an off-shell in-medium particle mismatches with the on-shell final states particle, which leads to the second term in  $\alpha_0$  in Eq. (12).

We then turn to the *first-order term*  $\mathcal{T}_{(1)}^{\mu\nu}$ , which is proportional to the hydrodynamic gradients and accounts for the off-equilibrium contribution induced by the system inhomogeneity.

Using the Zubarev’s formalism [47, 48], we obtain a Kubo formula at vanishing chemical potential that

$$W_{+(1)}^{\mu\nu} = \varepsilon_{\mathbf{p}} \lim_{\omega, q \rightarrow 0} \frac{\partial}{\partial \omega} [-\text{Im} G_{R+}^{\mu\nu\lambda\gamma}(\omega, \mathbf{q}, \mathbf{p})] \xi_{\lambda\gamma} \quad (13)$$

where the  $G_{R+}$  is embedded in retarded Green function

$$\begin{aligned} G_R^{\mu\nu\lambda\gamma}(t-t', \mathbf{x}, \mathbf{z}, \mathbf{y}) &\equiv \int \frac{d\omega}{2\pi} \frac{d^3\mathbf{q}}{(2\pi)^3} \frac{d^3\mathbf{p}}{(2\pi)^3} e^{-i\omega \cdot (t-t')} \\ &\quad \times e^{i\mathbf{q} \cdot (\mathbf{x}-\mathbf{z})} e^{i\mathbf{p} \cdot \mathbf{y}} G_R^{\mu\nu\lambda\gamma}(\omega, \mathbf{q}, \mathbf{p}) \\ &= (-i)\Theta(t-t') \langle [V^\mu(t, \mathbf{x}^-) V^\nu(t, \mathbf{x}^+), T^{\lambda\gamma}(t', \mathbf{z})] \rangle, \end{aligned} \quad (14)$$

and  $\xi_{\lambda\gamma} \equiv \beta^{-1} \partial_{(\lambda}(\beta u)_{\gamma)}$ . Combined with the ideal hydrodynamic equations,  $\xi_{\lambda\gamma}$  can be written as a linear combination of  $\sigma_{\lambda\gamma}$  and  $\theta$  at the leading gradient order as

$$\xi_{\lambda\gamma} \approx \sigma_{\lambda\gamma} + \left[ \frac{1}{3} \bar{\Delta}_{\lambda\gamma} + c_s^2 u_\lambda u_\gamma \right] \theta, \quad (15)$$

where  $c_s^2$  is the square of the sound speed, whose value at chemical freeze out, taken from lattice QCD data [49], is around 0.16. The shear part of the Kubo formula can also be obtained using metric variation in Ref [50, 51].

In Eq. (14),  $T^{\mu\nu} \equiv -F^\mu{}_\alpha F^{\nu\alpha} + m^2 V^\mu V^\nu - \eta^{\mu\nu} (-F^2/4 + m^2 V^2/2)$  stands for the Belinfante energy-momentum tensor of the sourceless Proca field, where  $F^{\mu\nu} \equiv \partial^\mu V^\nu - \partial^\nu V^\mu$ . After keeping only the leading order of the skeleton expansion[52–54], we express the  $G_R^{\mu\nu\lambda\gamma}(\omega, \mathbf{q}, \mathbf{p})$  in the medium rest frame as:

$$\begin{aligned} G_{R+}^{\mu\nu\lambda\gamma}(\omega, \mathbf{q}, \mathbf{p}) &= - \int_0^\infty dk_0 \int_0^\infty dk'_0 \frac{n(k'_0) - n(k_0)}{\omega + k'_0 - k_0 + i0^+} \\ &\quad \times \sum_{a,b=L,T} A_a(k) A_b(k') I_{ab}^{\mu\nu\lambda\gamma}(k, k'). \end{aligned} \quad (16)$$

The integral limits excluding the negative energy region allow us to conveniently select out the modes that are related to the physical modes in the Wigner functions. The neglected contribution is of high orders of  $\delta_{\text{qp}}$  defined later in the quasi-particle approximation schemes. With the projectors, the  $I_{ab}^{\mu\nu\lambda\gamma}(k, k')$  in Eq. (16) can be explicitly written as

$$\begin{aligned} I_{ab}^{\mu\nu\lambda\gamma}(k, k') &= [k^\lambda k'^\gamma + k^\gamma k'^\lambda] \Delta_a^{\nu\alpha}(k) \Delta_{b,\alpha}^{\mu\lambda}(k') \\ &\quad - [k_\alpha k'^\gamma \Delta_a^{\nu\lambda}(k) \Delta_b^{\mu\alpha}(k') + k^\gamma k'_\alpha \Delta_a^{\nu\alpha}(k) \Delta_b^{\mu\lambda}(k')] \\ &\quad - [k^\lambda k'_\alpha \Delta_a^{\nu\alpha}(k) \Delta_b^{\mu\gamma}(k') + k_\alpha k'^\lambda \Delta_a^{\nu\gamma}(k) \Delta_b^{\mu\alpha}(k')] \\ &\quad + (k_\alpha k'^\alpha - m^2) [\Delta_a^{\nu\lambda}(k) \Delta_b^{\mu\gamma}(k') + \Delta_a^{\nu\gamma}(k) \Delta_b^{\mu\lambda}(k')] \\ &\quad - \eta^{\gamma\lambda} [(k^\zeta k'_\zeta - m^2) \eta_{\alpha\beta} - k_\beta k'_\alpha] \Delta_a^{\nu\alpha}(k) \Delta_b^{\mu\beta}(k') \end{aligned} \quad (17)$$

where the  $k = (k_0, \mathbf{p} + \mathbf{q}/2)$ ,  $k' = (k'_0, \mathbf{p} - \mathbf{q}/2)$ .

To proceed further, we carry out the integration in the quasi-particle limit, i.e.,  $\Pi_{T,L}/\varepsilon_p^2 \sim \delta_{\text{qp}} \ll 1$ , so that all the integral over  $k_0$  and  $k'_0$  can be done in the vicinity of the pole of the propagator. Also, we assume the splitting is small, i.e.,  $(\Pi_L - \Pi_T)/(\Pi_L + \Pi_T) \sim \delta_{\text{sp}} \ll 1$ . Up to the (overall) zeroth order of  $\delta_\Gamma$  and  $\delta_{\text{sp}}$ , the off-shell contribution in the projectors in Eq.(16) can be neglected, and  $\mathcal{T}_{(1)}^{\mu\nu}$  can be simplified as

$$\mathcal{T}_{(1)}^{\mu\nu} = \beta n(\varepsilon_p) \bar{\Delta}_\lambda^{\langle\mu} \bar{\Delta}_\nu^{\rangle} [\alpha_{\text{sh}} \xi^{\gamma\lambda} + \alpha_{\text{sp}} \xi_p \frac{u^\lambda u^\gamma}{-\tilde{v}^2}] \quad (18)$$

where  $\xi_p = (\tilde{p}^\rho \tilde{p}^\sigma) \xi_{\rho\sigma} / \varepsilon_p^2$  and

$$\begin{aligned} \alpha_{\text{sh}} &= \frac{4\varepsilon_p \pi}{\beta n(\varepsilon_p)} \int_0^\infty \frac{\partial n(\omega)}{\partial \omega} d\omega (\omega^2 - \varepsilon_p^2) A_{T/L}^2(\omega, \mathbf{p}) \quad (19) \\ \alpha_{\text{sp}} &= \frac{4\varepsilon_p \pi}{\beta n(\varepsilon_p)} \int_0^\infty \frac{\partial n(\omega)}{\partial \omega} d\omega \varepsilon_p^2 (A_T^2(\omega, \mathbf{p}) - A_L^2(\omega, \mathbf{p})). \end{aligned}$$

Furthermore, in quasi-particle limits, the spectral function nearby the positive frequency pole can be approximately expressed as

$$A_a(\omega, \mathbf{p}) \approx \frac{1}{2\varepsilon_p} \frac{1}{\pi} \text{Im} \frac{-1}{\omega - \omega_p^a + i\Gamma_p^a/2} \quad (20)$$

where  $\Gamma_p^a = \text{Im}\Pi_a(\omega_p^a, \mathbf{p})/\varepsilon_p$  is the width. With an expansion of  $\partial n(\omega)/\partial \omega$  to the first order of  $\Delta\omega/T$  as  $\propto n(\varepsilon_p)(1 - \Delta\omega/T)$  [55],  $\alpha_{\text{sh}}$  and  $\alpha_{\text{sp}}$  can be further simplified as [56]

$$\begin{aligned} \alpha_{\text{sh}} &\approx -\frac{2\Delta\varepsilon_p}{\Gamma_p} + 2\frac{\Delta\varepsilon_p}{\Gamma_p} \frac{\Delta\varepsilon_p}{T} + \frac{\Gamma_p}{2T} \sim \mathcal{O}(1) \quad (21) \\ \alpha_{\text{sp}} &\approx -\frac{\varepsilon_p}{\Gamma_p} \left( \frac{\Gamma_p^\Delta}{\Gamma_p} - \frac{\Delta\varepsilon_p}{T} \frac{\Gamma_p^\Delta}{\Gamma_p} + \frac{\Gamma_p}{T} \frac{\omega_p^\Delta}{\Gamma_p} \right) \sim \mathcal{O}(\delta_{\text{qp}}^{-1} \delta_{\text{sp}}). \end{aligned}$$

with  $\Gamma_p^\Delta \equiv \Gamma_p^L - \Gamma_p^T$  and  $\omega_p^\Delta \equiv \omega_p^L - \omega_p^T$  being the difference between the width and dispersion relations of the  $L$  and  $T$  modes.  $\Delta\varepsilon_p$  and  $\Gamma_p$  are defined as  $\Delta\varepsilon_p = \omega_p^{L/T} - \varepsilon_p$  and  $\Gamma_p = \Gamma_p^{L/T}$ , where the differences caused by choosing  $L/T$  are  $\mathcal{O}(\delta_{\text{sp}})$ . Also, the Bose enhancement factors in Eq. (21) are neglected since  $n(\varepsilon_p)$  is small for vector boson with large mass. Finally, to make the obtained  $\alpha_{\text{sh}}$  and  $\alpha_{\text{sp}}$  covariant, we need to replace  $\mathbf{p}$  with  $\mathbf{p}_\perp^\mu \equiv \bar{\Delta}^{\mu\nu} p_\nu$  and  $\varepsilon_p$  with  $\varepsilon_0 \equiv \tilde{p} \cdot u$ .

After comparing Eq. (12) and Eq. (18) with Eq.(9), we obtain the  $\kappa$ -parameters at current order as

$$\begin{aligned} \kappa_0^u &= \frac{\alpha_0}{-\tilde{v}^2} n_0, \quad \kappa_1^u = \left[ \alpha_{\text{sh}} \left( c_s^2 - \frac{1}{3} \right) \theta + \frac{\alpha_{\text{sp}} \xi_p}{-\tilde{v}^2} \right] \beta n_0 \\ \kappa_{\text{sh}} &= \alpha_{\text{sh}} \beta n_0, \quad \kappa_T = 0, \quad \kappa_{\text{su}} = 0, \quad \kappa_{\text{ou}} = 0 \end{aligned} \quad (22)$$

with  $n_0 = n(\varepsilon_0)$ . The  $\alpha_0$  is at least of first order in  $\delta_{\text{sp}/\text{qp}}$  but of zeroth order in  $\partial$ . Thus,  $\mathcal{T}$  in this multi-parameter expansion is at the first order of  $\partial$ ,  $\delta_{\text{sp}}$  or  $\delta_{\text{qp}}$ . For higher orders, there are non-vanishing contributions from  $\kappa_{\text{su}} \propto \delta_{\text{sp}/\text{qp}}$  and  $\kappa_T \propto$  ‘‘high order gradients’’, while  $\kappa_{\text{ou}}$  could be nonzero with asymmetric  $T^{\mu\nu}$ .

Some relevant and interesting physics other than tensor polarization can be studied under the similar formalism. For example, the vector polarization for vector boson can be proven equal to 4/3 of the one for spin-1/2 particle as expected. However, due to the limited space, we would leave such discussions together with more details of the present work to our long paper [57].

*Implications for phenomenologies.*—We then discuss the phenomenological implication of the theoretical findings, in which we take the commonly used freezeout assumption for spin physics [21, 23, 58]. Within this assumption, vector meson’s spin alignment stops to evolve

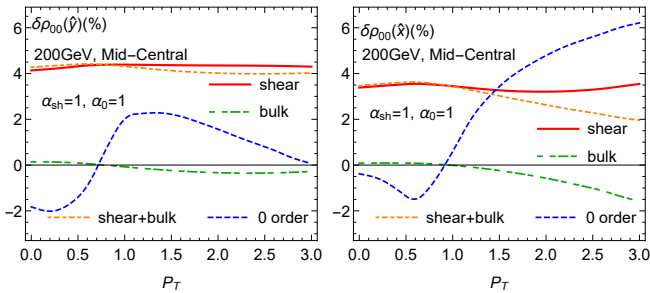


FIG. 1. The effects of the first three contributions (“0 order”, “bulk”, “shear”) in Eq. (9) with  $\hat{y}$  (left) and  $\hat{x}$  (right) as quantization axis and  $\alpha_0 = \alpha_{\text{sh}} = 1$ . The final results should be scaled by the physical value of  $\alpha_0$  and  $\alpha_{\text{sh}}$ .

at certain freezeout temperature (or other freezeout conditions), where a Cooper-Fry like formula for the spin alignment  $\delta\rho_{00}$  can be written with the tensor polarization  $\mathcal{T}^{\mu\nu}$  as

$$\delta\rho_{00}(\hat{n}_{\text{pr}}, \mathbf{p}) = \frac{\int d\Sigma^\lambda p_\lambda \mathcal{T}^{\mu\nu}(x, \mathbf{p}) \hat{n}_\mu(\mathbf{p}) \hat{n}_\nu(\mathbf{p})}{d\Sigma^\lambda p_\lambda \mathcal{S}(x, \mathbf{p})}. \quad (23)$$

The  $\Sigma^\lambda$  is the hyper-surface satisfying the freeze-out condition, and  $\hat{n}^\mu$  is a shorthand of  $\epsilon_{s=0}^\mu$ , which is related to a 3d unit vector  $\hat{n}_{\text{pr}}$  by a Lorentz boost, i.e.,  $\hat{n}^\mu = [\Lambda(\mathbf{p}) \cdot \hat{n}_{\text{pr}}]^\mu$ , with  $\hat{n}_{\text{pr}}$  being the polarization vector  $\epsilon_{s=0, \text{pr}}^\mu$  in the particle rest frame. In a realistic measurement,  $\hat{n}_{\text{pr}}$  is usually taken either in the in-plane ( $\hat{x}$ ) or out-plane ( $\hat{y}$ ) direction. The scalar contribution  $\mathcal{S}(x, \mathbf{p})$  on the denominator is approximately equal to three times of the particle number density.

The hydrodynamic profile is taken from the previous work [21] using CLVisc [18] with a freeze-out temperature at 157 MeV and the AMPT initial condition [21] for Au-Au collisions at mid-centrality, where the impact parameter is around 9 fm. For the illustrative purpose, we take  $\alpha_0 = 1$ , which could be significantly over estimated since  $\alpha_0 \sim \mathcal{O}(\delta_{\text{sp}/\text{qp}})$ ,  $\alpha_{\text{sh}} = 1$ ,  $m = 1$  GeV, and  $\alpha_{\text{sp}} = 0$  [59]. The first three contributions from Eq. (9) to the spin alignment  $\delta\rho_{00}$  obtained with  $\hat{n}_{\text{pr}}$  chosen as both  $\hat{x}$  and  $\hat{y}$  are plotted with respect to  $p_T$  in Fig. (1). As shown in Fig. 1, with an  $\alpha_{\text{sh}}$  approximately ranging from 0.1 to 1 (estimated using the light or heavy meson’s spectral properties in Ref [60–64]), the SITP alone would contribute to the spin alignment with the magnitude around 1%, which is not that far from those observed in experiments. Given a positive  $\alpha_{\text{sh}}$ , and the fact that usually  $\partial_z u^z > \partial_x u^x > \partial_y u^y$  in a high energy non-central HICs, we get  $\sigma_{yy} > 0$ ,  $\sigma_{yy} > \sigma_{xx}$ , and hence  $\rho_{00}^{\text{SITP}}(\hat{y}) > 0$ ,  $\rho_{00}^{\text{SITP}}(\hat{y}) > \rho_{00}^{\text{SITP}}(\hat{x})$ , which is consistent with the trends shown in Fig. 1. Similar analysis can be applied to the  $u^\mu u^\nu$  term to understand its dependence on  $p_T$  and  $\hat{n}_{\text{pr}}$ .

Besides the dependence on the hydrodynamic gradients, the behaviors of spin alignment highly are affected by the behaviors of coefficients in Eq. (9) as well. These

coefficients can have nontrivial momentum dependencies and are further determined by the vector meson’s spectral properties or say microscopic interactions in medium, which could be significantly different at different temperatures, phases, and etc. Thus, the coefficients are sensitive to the freeze-out moment in various freeze-out scenarios. For  $J/\psi$ , it can form and freeze-out in quark-gluon plasma (QGP). For  $\phi$  meson, it can emerge in QGP [63–65]. Since its width and relaxation time is uncertain [60–62, 66–69], it can freeze-out at the late stage of QGP, early hadronic phase, or even around the kinetic freeze-out if the hadronic phase is long enough. For  $K^*$  meson, the situation can again be different from  $\phi$  meson [37]. On the other hand, one should note that as the kinetic freeze-out time [70] and temperature [71] are different in different collision beam energies and centralities, they could also make “freeze-out” scenario different. These rich physics are probably helpful to explain the diverse behaviors observed in various experiments [30, 32, 33]. Meanwhile, taking the advantage of the experimental progresses, we can also utilize the measured data to reversely probe the rich physics of medium, such as in-medium spectral properties and microscopic interactions.

As described above, the spin alignment discovered in HICs could be influenced by the rich physics in a multi-phase evolution, which are beyond the scope of this paper. Thus, in the following, we just focus on the spin alignment in QGP phase, where some qualitative conclusions can be obtained based on the spectral properties discussed in Ref [63, 64]. At the  $T \sim 200$  MeV, the in-medium width of the regenerated  $J/\psi$  can be at an order of 100 MeV [64, 72], while those of the light meson resonances could be even broader [64]. Therefore, at least, in the QGP stage, vector meson can have a  $\alpha_{\text{sh}}$  more than  $\Gamma_{\mathbf{p}}/(2T) \sim 0.3$  leading to a spin alignment at 1% order with a positive sign [73], which is qualitatively similar to those observed at RHIC experiment [33] and is of the opposite sign of  $J/\psi$ ’s spin alignment at ALICE [74].

*Summary.*—In summary, we have conducted the first thermal field theory calculation on the tensor polarization and spin alignment of vector meson up to first order in gradient, which leads to three theoretical findings. First, the tensor polarization, and hence the spin alignment, of a massive vector boson are found to be nonzero at the zeroth-order in gradient expansion mainly due to the degeneracy breaking between the longitudinal and transverse modes. Second, at the first order of the hydrodynamics gradient, we discover several new mechanisms generating the tensor polarization and spin alignment including SITP. Third, the tensor polarization and spin alignment are found to be closely related to the spectral properties and hence the microscopic interactions among the vector bosons.

For the phenomenology, we find that SITP could lead to the spin alignment of order 1%, if the in-medium in-

interaction generate relatively large width/collisions rates or/and large mass-shift. Meanwhile, various  $p_T$  dependencies from several different contributions and rich physics of the medium interactions encoded in coefficients can potentially provide an explanation to the rich and intriguing experimental data. On the other hand, the studies also suggest that the spin alignment phenomena can potentially be reversely used as a probe to spectral properties of vector bosons in-medium.

In future, we will further improve the theoretical derivation with a more sophisticated microscopic calculations of the in-medium spectral properties of the vector mesons. Meanwhile, we shall employ a better quantitative phenomenology model that can accommodate the non-equilibrium effects and other novel effects proposed in Ref [38, 75]. Additionally, the presence of the newly discovered SITP effect is robust against the variation of the details of the interactions and universal in both relativistic and non-relativistic cases. Therefore, it should be interesting to seek it experimentally in low energy physics, such as plasma physics or cold atom physics[76].

**Acknowledgments** We gratefully acknowledge the valuable contribution from Yi Yin, who definitely deserves a key position in the author list, but waive the authorship generously. We also especially thanks Long-gang Pang who provides hydrodynamic profiles for numerical studies. We thank Hengtong Ding, Xiaojian Du, Aiqiang Guo, Koichi Hattori, Min He, Che-Ming Ko, Yutie Liang, Shu Lin, Rapp Ralf, Kaijia Sun, Subhash Singha, Shuzhe Shi, Yifeng Sun, Aihong Tang, Biaogang Wu, Dilun Yang, Wenbin Zhao for valuable discussions. FL is supported by NSFC No. 12105129. SL is supported by Fundamental Research Funds for the central Universities.

---

\* fengli@lzu.edu.cn

† Corresponding author.

lshphy@hnu.edu.cn

- [1] C. Bourrely, J. Soffer, and E. Leader, Phys. Rept. **59**, 95 (1980).
- [2] M. I. Haftel, L. Mathelitsch, and H. F. K. Zingl, Phys. Rev. C **22**, 1285 (1980).
- [3] R. J. Holt, J. R. Specht, K. Stephenson, B. Zeidman, J. S. Frank, M. J. Leitch, J. D. Moses, E. J. Stephenson, and R. M. Laszewski, Phys. Rev. Lett. **47**, 472 (1981).
- [4] M. E. Schulze *et al.*, Phys. Rev. Lett. **52**, 597 (1984).
- [5] D. Abbott *et al.* (JLAB t(20)), Phys. Rev. Lett. **84**, 5053 (2000), arXiv:nucl-ex/0001006.
- [6] K.-b. Chen, W.-h. Yang, S.-y. Wei, and Z.-t. Liang, Phys. Rev. D **94**, 034003 (2016), arXiv:1605.07790 [hep-ph].
- [7] K.-b. Chen, Z.-t. Liang, Y.-k. Song, and S.-y. Wei, Phys. Rev. D **102**, 034001 (2020), arXiv:2002.09890 [hep-ph].
- [8] L. Adamczyk *et al.* (STAR), Nature **548**, 62 (2017).
- [9] J. Adam *et al.* (STAR), Phys. Rev. C **98**, 014910 (2018), arXiv:1805.04400 [nucl-ex].
- [10] T. Niida (STAR), Nucl. Phys. A **982**, 511 (2019).
- [11] J. Adam *et al.* (STAR), Phys. Rev. Lett. **123**, 132301 (2019), arXiv:1905.11917 [nucl-ex].
- [12] S. Acharya *et al.* (ALICE), Phys. Rev. Lett. **128**, 172005 (2022), arXiv:2107.11183 [nucl-ex].
- [13] Z.-T. Liang and X.-N. Wang, Phys. Rev. Lett. **94**, 102301 (2005), [Erratum: Phys. Rev. Lett.96,039901(2006)].
- [14] F. Becattini, V. Chandra, L. Del Zanna, and E. Grossi, Annals Phys. **338**, 32 (2013).
- [15] I. Karpenko and F. Becattini, Eur. Phys. J. C **77**, 213 (2017), arXiv:1610.04717 [nucl-th].
- [16] H. Li, L.-G. Pang, Q. Wang, and X.-L. Xia, Phys. Rev. C **96**, 054908 (2017), arXiv:1704.01507 [nucl-th].
- [17] Y. Sun and C. M. Ko, Phys. Rev. C **96**, 024906 (2017).
- [18] L.-G. Pang, H. Petersen, Q. Wang, and X.-N. Wang, Phys. Rev. Lett. **117**, 192301 (2016).
- [19] S. Y. F. Liu, Y. Sun, and C. M. Ko, Phys. Rev. Lett. **125**, 062301 (2020), arXiv:1910.06774 [nucl-th].
- [20] S. Y. F. Liu and Y. Yin, JHEP **07**, 188 (2021), arXiv:2103.09200 [hep-ph].
- [21] B. Fu, S. Y. F. Liu, L. Pang, H. Song, and Y. Yin, Phys. Rev. Lett. **127**, 142301 (2021), arXiv:2103.10403 [hep-ph].
- [22] F. Becattini, M. Buzzegoli, and A. Palermo, Phys. Lett. B **820**, 136519 (2021), arXiv:2103.10917 [nucl-th].
- [23] F. Becattini, M. Buzzegoli, G. Inghirami, I. Karpenko, and A. Palermo, Phys. Rev. Lett. **127**, 272302 (2021), arXiv:2103.14621 [nucl-th].
- [24] B. Fu, L. Pang, H. Song, and Y. Yin, (2022), arXiv:2201.12970 [hep-ph].
- [25] X.-Y. Wu, C. Yi, G.-Y. Qin, and S. Pu, (2022), arXiv:2204.02218 [hep-ph].
- [26] Z.-T. Liang and X.-N. Wang, Phys. Lett. B **629**, 20 (2005), arXiv:nucl-th/0411101.
- [27] S. A. Voloshin, (2004), arXiv:nucl-th/0410089.
- [28] F. Becattini, F. Piccinini, and J. Rizzo, Phys. Rev. C **77**, 024906 (2008), arXiv:0711.1253 [nucl-th].
- [29] B. I. Abelev *et al.* (STAR), Phys. Rev. C **77**, 061902 (2008), arXiv:0801.1729 [nucl-ex].
- [30] S. Acharya *et al.* (ALICE), Phys. Rev. Lett. **125**, 012301 (2020), arXiv:1910.14408 [nucl-ex].
- [31] S. Singha (STAR), Nucl. Phys. A **1005**, 121733 (2021), arXiv:2002.07427 [nucl-ex].
- [32] (2022), arXiv:2204.10171 [nucl-ex].
- [33] M. S. Abdallah *et al.* (STAR), Nature **614**, 244 (2023), arXiv:2204.02302 [hep-ph].
- [34] F. Becattini and F. Piccinini, Annals Phys. **323**, 2452 (2008), arXiv:0710.5694 [nucl-th].
- [35] X.-L. Xia, H. Li, X.-G. Huang, and H. Zhong Huang, Phys. Lett. B **817**, 136325 (2021), arXiv:2010.01474 [nucl-th].
- [36] F. Becattini, (2022), arXiv:2204.01144 [nucl-th].
- [37] X.-L. Sheng, L. Oliva, and Q. Wang, Phys. Rev. D **101**, 096005 (2020), arXiv:1910.13684 [nucl-th].
- [38] B. Müller and D.-L. Yang, (2021), 10.1103/PhysRevD.105.L011901, arXiv:2110.15630.
- [39] N. Weickgenannt, D. Wagner, and E. Speranza, (2022), arXiv:2204.01797 [nucl-th].
- [40] X.-L. Sheng, L. Oliva, Z.-T. Liang, Q. Wang, and X.-N. Wang, (2022), arXiv:2206.05868 [hep-ph].
- [41] F. Becattini and I. Karpenko, Phys. Rev. Lett. **120**, 012302 (2018).
- [42] There are subtleties on this relation, but they will not will not affects symmetric parts of  $\mathcal{W}^{\mu\nu}$  [77].
- [43] C. Gale and J. I. Kapusta, Nucl. Phys. B **357**, 65 (1991).

- [44] R. Rapp, G. Chanfray, and J. Wambach, Nucl. Phys. A **617**, 472 (1997), arXiv:hep-ph/9702210.
- [45] G. Baym, T. Hatsuda, and M. Strickland, Phys. Rev. C **95**, 044907 (2017), arXiv:1702.05906 [nucl-th].
- [46] E. Speranza, A. Jaiswal, and B. Friman, Phys. Lett. B **782**, 395 (2018), arXiv:1802.02479 [hep-ph].
- [47] A. Hosoya, M.-a. Sakagami, and M. Takao, Annals Phys. **154**, 229 (1984).
- [48] D. N. Zubarev, *Nonequilibrium statistical thermodynamics* (Consultants Bureau, 1974).
- [49] S. Borsanyi, Z. Fodor, C. Hoelbling, S. D. Katz, S. Krieg, and K. K. Szabo, Phys. Lett. B **730**, 99 (2014), arXiv:1309.5258 [hep-lat].
- [50] J. M. Luttinger, Phys. Rev. **135**, A1505 (1964).
- [51] G. D. Moore and K. A. Sohrabi, Phys. Rev. Lett. **106**, 122302 (2011), arXiv:1007.5333 [hep-ph].
- [52] M. Srednicki, *Quantum field theory* (Cambridge University Press, 2007).
- [53] F. J. Dyson, Phys. Rev. **75**, 1736 (1949).
- [54] J. M. Luttinger and J. C. Ward, Phys. Rev. **118**, 1417 (1960).
- [55] Error is not too large for relatively large  $\Delta\omega/T$ . For  $\Gamma_p/T(\varepsilon_p/T) \sim 0.5$ , the error is around 20%.
- [56] Useful identities:  $\int dx x^2(c/((x)^2 + c^2))^2 = \pi c/2$ ,  $\int dx(c/(x^2 + c^2))^2 = \pi/(2c)$ .
- [57] S. Y. F. Liu and F. Li, in preparation (2022).
- [58] F. Becattini, G. Cao, and E. Speranza, Eur. Phys. J. C **79**, 741 (2019), arXiv:1905.03123 [nucl-th].
- [59] If  $\alpha_{sp} = 1$ , the contribution is at the order of  $\pm 0.2\%$ .
- [60] R. Rapp, Phys. Rev. C **63**, 054907 (2001), arXiv:hep-ph/0010101.
- [61] H. van Hees and R. Rapp, Nucl. Phys. A **806**, 339 (2008), arXiv:0711.3444 [hep-ph].
- [62] G. Vujanovic, J. Ruppert, and C. Gale, Phys. Rev. C **80**, 044907 (2009), arXiv:0907.5385 [nucl-th].
- [63] S. Y. F. Liu and R. Rapp, Eur. Phys. J. A **56**, 44 (2020), arXiv:1612.09138 [nucl-th].
- [64] S. Y. F. Liu and R. Rapp, Phys. Rev. C **97**, 034918 (2018).
- [65] E. V. Shuryak and I. Zahed, Phys. Rev. D **70**, 054507 (2004).
- [66] K. L. Haglin and C. Gale, Nucl. Phys. B **421**, 613 (1994), arXiv:nucl-th/9401003.
- [67] C. Song, Phys. Lett. B **388**, 141 (1996), arXiv:hep-ph/9603259.
- [68] S. Pal, C. M. Ko, and Z.-w. Lin, Nucl. Phys. A **707**, 525 (2002), arXiv:nucl-th/0202086.
- [69] C. M. Ko, V. Koch, and G.-Q. Li, Ann. Rev. Nucl. Part. Sci. **47**, 505 (1997), arXiv:nucl-th/9702016.
- [70] B. Wu, X. Du, M. Sibila, and R. Rapp, Eur. Phys. J. A **57**, 122 (2021), [Erratum: Eur.Phys.J.A 57, 314 (2021)], arXiv:2006.09945 [nucl-th].
- [71] L. Adamczyk *et al.* (STAR), Phys. Rev. C **96**, 044904 (2017), arXiv:1701.07065 [nucl-ex].
- [72] M. He, B. Wu, and R. Rapp, Phys. Rev. Lett. **128**, 162301 (2022), arXiv:2111.13528 [nucl-th].
- [73] We also checked directly with  $m = 3$  GeV.
- [74] S. Acharya *et al.* (ALICE), Phys. Rev. Lett. **131**, 042303 (2023), arXiv:2204.10171 [nucl-ex].
- [75] X.-L. Sheng, L. Oliva, Z.-T. Liang, Q. Wang, and X.-N. Wang, Phys. Rev. Lett. **131**, 042304 (2023), arXiv:2205.15689 [nucl-th].
- [76] P. D. Gregory, J. A. Blackmore, J. Aldegunde, J. M. Hutson, and S. L. Cornish, Phys. Rev. A **96**, 021402 (2017).
- [77] K. Hattori, Y. Hidaka, N. Yamamoto, and D.-L. Yang, (2020), 10.1007/jhep02(2021)001.
- [78] W.-B. Dong, Y.-L. Yin, X.-L. Sheng, S.-Z. Yang, and Q. Wang, (2023), arXiv:2311.18400 [hep-ph].
- [79] M. Buballa, Phys. Rept. **407**, 205 (2005), arXiv:hep-ph/0402234.
- [80] F. Li, *Spinodal Instabilities in NJL and PNJL Model*, Ph.D. thesis, Texas A-M (2016).

## SUPPLEMENTAL MATERIAL

In this supplemental material, we will show the potential capability of our theory to generate nontrivial  $p_T$  and centrality dependence of the spin alignment under certain assumptions.

We first evaluate the coefficients  $\alpha_0$ ,  $\alpha_{sh}$  and  $\alpha_{sp}$  numerically according to Eq. (12) and (19) for  $\phi$  meson with in-medium spectral functions obtained via a 1-loop quark meson model calculation as discussed in Ref. [78]. These coefficients are plotted in Fig. 2 for the cases with the effective strange quark masses  $m_s = \{0.3, 0.42, 0.5\}$  GeV. The purpose for choosing various masses will be discussed later. As shown in Fig. 2,  $\alpha_{sh}$  decreases from positive to negative as  $p_T$  increases for the cases with  $m_s = 0.3$  and 0.42 GeV. This can be understood, according to Eq. (21), as a result of the competition between a positive  $\Gamma_{\mathbf{p}}/(2T)$  and a negative  $-2\Delta\varepsilon_{\mathbf{p}}/\Gamma_{\mathbf{p}}$ . Since both  $\Delta\varepsilon_{\mathbf{p}}$  and  $\Gamma_{\mathbf{p}}$  are suppressed by a factor  $m_\phi/\varepsilon_{\mathbf{p}}$ ,  $-2\Delta\varepsilon_{\mathbf{p}}/\Gamma_{\mathbf{p}}$  with this factor canceled, should take over  $\Gamma_{\mathbf{p}}/(2T)$  at large momenta and reduces  $\alpha_{sh}$  from positive to negative. For  $m_s = 0.5$  GeV,  $\phi$  meson mass is so close to  $2m_s$  threshold that  $\Gamma_{\mathbf{p}}$  becomes much smaller, making  $\Gamma_{\mathbf{p}}/(2T) < 2\Delta\varepsilon_{\mathbf{p}}/\Gamma_{\mathbf{p}}$  and  $\alpha_{sh}$  negative for all momenta.

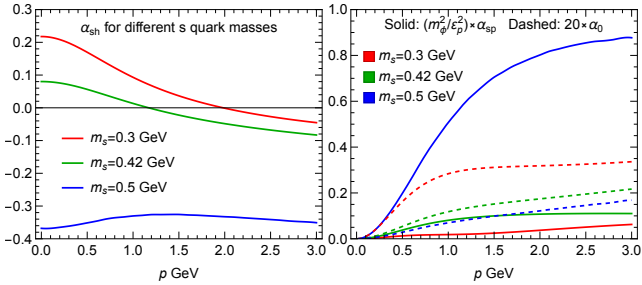


FIG. 2. Momentum dependence of the  $\alpha_{sh}$ ,  $(m_\phi^2/\varepsilon_p^2) \times \alpha_{sp}$  and  $20 \times \alpha_0$  with different  $s$  quark masses.

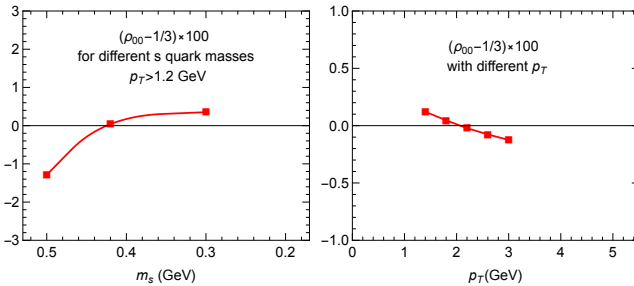


FIG. 3.  $\delta\rho_{00}(\hat{y})$  as a function of  $m_s$  (left), and of  $p_T$  for  $m_s = 0.42$  GeV (right). The  $m_s$  dependence might be related to the centrality dependence under certain assumptions.

With these coefficients, we further calculate  $\delta\rho_{00}$  with

the hydrodynamic profiles used before, whose general trend is found mainly controlled by the SITP effect. As shown in Fig. 3, the  $\delta\rho_{00}$  decreases with  $p_T$  from positive to negative, which is similar to the experimental measurements in Ref. [33], and can be understood from the shear contribution, approximately proportional to  $\alpha_{sh}(\partial_z u_z + \partial_x u_x - 2\partial_y u_y)$ . The shear tensor should be positive since  $\partial_z u_z > \partial_x u_x \geq \partial_y u_y > 0$  in high energy HICs. The  $p_T$  dependence of the shear contribution, and hence of  $\delta\rho_{00}$ , could be originated naturally from the momentum dependence of  $\alpha_{sh}$ , which, as illustrated by the green curve in the left panel of Fig. 2, decreases with momentum from positive to negative. Similarly, the negative  $m_s$  dependence of  $\delta\rho_{00}$  shown in the left panel in Fig. 3 can be understood from the shear contribution as well, since  $\alpha_{sh}$  also decreases with  $m_s$  from positive to negative at low and middle momenta as shown in Fig. 2.

The obtained  $m_s$  dependence of  $\delta\rho_{00}$  could resemble the observed centrality dependence shown in Ref. [33], if we assume the mapping between  $m_s$  and centrality as: “0.5 GeV  $\leftrightarrow$  0–20%”, “0.42 GeV  $\leftrightarrow$  20–40%”, and “0.3 GeV  $\leftrightarrow$  40–60%”. Such a mapping is possible, if the spin-alignments freeze-out at higher temperatures for larger centralities (more peripheral), similar to the trend observed at kinetic freeze-out in Ref. [71]. This positive dependence of the freeze-out temperature on the centrality might be understandable given the centrality dependence of the fireball lifetime shown in Ref. [70]. Colliding systems with larger centralities might be so short-lived that there is not enough time for the late-stage collisions to occur so that the freeze-out happens earlier with higher temperatures. Meanwhile, the effective  $s$  quark mass, or the mass of alternative constituents (such as kaons in hadronic phases) of  $\phi$  meson, might drop with temperature within a narrow window close to the QCD phase boundary, either due to chiral symmetry restoration as demonstrated in Ref. [79, 80], or due to the exhibition of the low lying collective modes in QGP originated from non-condensate interactions as shown in Ref. [64]. Similar physics could also be relevant to the understandings of the different spin alignments at different beam energies.

In summary, under certain assumptions, the nontrivial sign flipping behavior observed in the  $p_T$  and centrality dependencies of spin alignment emerge naturally with the SITP effect, exhibiting its promising capability to describe the rich behaviors of spin alignment observed in experiments. This toy-model like exploration definitely oversimplifies the rich in-medium physics of vector mesons and many phenomenological setups. More sophisticated and systematic studies are in progress and will be reported in a series of upcoming papers.